Optics Letters

Photonics-enabled simultaneous self-interference cancellation and image-reject mixing

DAN ZHU, XIAOPENG HU, WENJUAN CHEN, DE BEN, AND SHILONG PAN*

Key Laboratory of Radar Imaging and Microwave Photonics, Ministry of Education, Nanjing University of Aeronautics and Astronautics, Nanjing 210016, China
*Corresponding author: pans@nuaa.edu.cn

Received 6 September 2019; revised 21 October 2019; accepted 21 October 2019; posted 23 October 2019 (Doc. ID 377192); published 11 November 2019

Both self-interference and image interference are key practical impediments to realize in-band full-duplex radio-frequency (RF) systems. The previous photonics-based approaches can realize either self-interference cancellation or image-reject mixing. The only approach to realize both functions relies on electrical operations of phase shift, power weighting, and time delay, leading to limited bandwidth and frequency. This Letter proposes and demonstrates a photonic approach to realize simultaneous self-interference cancellation and image-reject mixing. The key is that by introducing only one polarization-multiplexed 90° optical hybrid, simultaneous 0, π, $\pi/2$, and $3\pi/2$ phase shifts can be introduced in the optical domain. In addition, power weighting and time delay of the reference signal for self-interference cancellation can be realized in the optical domain with the help of polarization multiplexing. In this way, all the operations required by both functions are realized using optical methods. Both theoretical and experimental investigations are performed. Simultaneous self-interference cancellation and image-reject mixing are achieved, with a self-interference cancellation depth of 35 dB over 100-MHz bandwidth, 24 dB over 400-MHz bandwidth, and 18 dB over 1-GHz bandwidth in the X and Ku bands, and an image-rejection ratio larger than 53 dB over 1-GHz bandwidth in the X band.

https://doi.org/10.1364/OL.44.005541

A global challenge for future radio-frequency (RF) systems is to develop new functions and services covering broad bandwidth while the available spectrum is limited [1–3]. The capabilities of in-band full-duplex communication and spectral efficiency improvement are highly required in future radio systems for wireless communications, frequency-modulated continuous-wave radar, and electronic warfare [4–6]. Two important functions of self-interference cancellation and image-reject mixing are therefore urgently needed. The self-interference refers to the unwanted signal leaked from the transmitter to its own receiver. Meanwhile, the image refers to the unwanted signal at ω_j that will be downconverted to the same intermediate frequency (IF) band of $\omega_{IF} = |\omega_{RF} - \omega_{LO}|$ when the wanted RF signal of ω_{RF} is mixed with a local oscillator (LO) signal at ω_{LO} [7]. Both the self-interference and image have the in-band spectrum aliasing with the wanted RF signal, which cannot be eliminated simply through filtering.

Many approaches have been proposed to realize either self-interference cancellation or image-reject mixing. To realize self-interference cancellation, photonics-based approaches have been widely investigated thanks to the advantages of wide bandwidth, parallel signal processing and low transmission loss introduced by photonics [8–13]. The basic idea is to introduce a small portion of the transmitted signal (or reference signal) to the receiver. The received RF signal (containing the interference) and the reference signal are modulated to the optical domain, respectively. The optically carried reference signal is properly delayed, power weighted, phase inverted, and then combined with the optically carried RF signal, by which the interference in the received signal is canceled. For the previous photonic self-interference cancellation approaches, the main point is focused on realizing the phase inversion via balanced photodetection [10], counterbiasing modulations [11], phase modulation (i.e., using the out-of-phase property of the phase-modulated sidebands) [12], or using a microwave photonic phase shifter to adjust the phase of one signal [13].

On the other hand, image-reject mixing based on microwave photonics has been intensively studied to suppress the image interference [14–18]. Typically, Hartley architecture is applied to suppress the image interference without employing prefiltering. In this architecture, two quadrature IF outputs are generated through mixing a pair of quadrature LO (or RF) signals with the RF (or LO) signal, which are combined after introducing an additional $\pi/2$-phase difference. The downconverted RF signal is in phase and enhanced, while the downconverted image is out of phase and eliminated. However, for all the above approaches, only one function can be realized. To the best of our knowledge, the simultaneous self-interference cancellation and image-reject mixing is only achieved in Ref. [19]. The structure is simple. However, this approach relies on electrical operations of the phase shift of the LO signal, and the power weighting and time delay of the reference, leading to limited bandwidth and frequency.

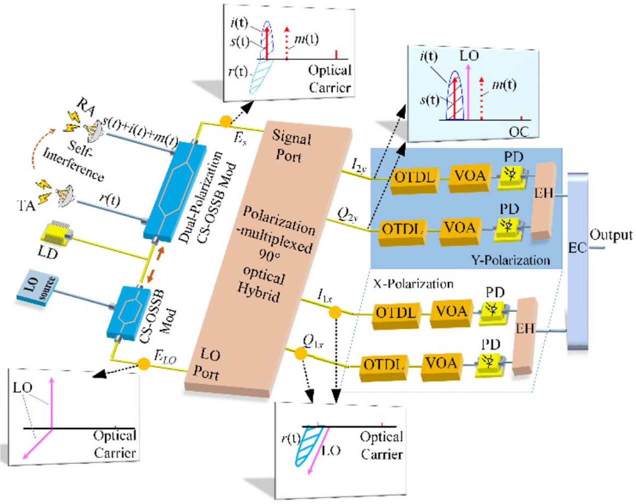

Fig. 1. Schematic diagram of simultaneous self-interference cancellation and image-reject mixing based on a polarization-multiplexed 90° optical hybrid. LD, laser diode; PC, polarization controller; CS-OSSB Mod, carrier-suppressed optical single-sideband modulator; OBPF, optical bandpass filter; OTDL, optical tunable delay line; VOA, variable optical attenuator; LO, local oscillator; PD, photodetector; EH, electrical hybrid; EC, electrical coupler.

Recently, we have proposed a photonic approach to realize simultaneous self-interference cancellation and image-reject mixing based on a polarization-multiplexed 90° optical hybrid [20]. But, it only reported some preliminary experimental results. In order to understand the approach in detail, a comprehensive investigation is performed in this Letter. The key is that by introducing only one polarization-multiplexed 90° optical hybrid, 0, π, $\pi/2$, and $3\pi/2$ phase shifts can be introduced in the optical domain simultaneously. In addition, the power weighting and time delay of the reference signal for self-interference cancellation are realized in the optical domain with the help of polarization multiplexing. Simultaneous self-interference cancellation and image-reject mixing are achieved, with a self-interference cancellation depth of 35 dB over 100 MHz bandwidth, 24 dB over 400 MHz bandwidth, and 18 dB over 1 GHz bandwidth in the X and Ku bands, and an image-rejection ratio larger than 53 dB over 1 GHz bandwidth in the X band.

The schematic diagram of the proposed photonic scheme for simultaneous self-interference cancellation and image-reject mixing is shown in Fig. 1. A light wave with the angular frequency of ω_c is split into two parts. One part is injected into a dual-polarization carrier-suppressed optical single-sideband (CS-OSSB) modulator. The received RF signal and a reference signal are modulated to the same optical carrier with orthogonal polarization states, and the modulation format is set to be CS-OSSB modulation. The received RF signal consists of the signal of interest $s(t) = V_s \sin(\omega_s t)$, the image $m(t) = V_m \sin(\omega_m t)$, and the self-interference $i(t) = V_i \sin(\omega_r t)$, while $r(t) = V_r \sin(\omega_r t)$ represents the reference signal. The output of the dual-polarization CS-OSSB modulator can be written as

$$\begin{aligned} E_s &= \hat{e}_x \cdot E_{\mathrm{RF}x} + \hat{e}_y \cdot E_{\mathrm{RF}y} \\ &= \hat{e}_x \cdot \{a_s e^{j(\omega_c-\omega_s)t} + a_m e^{j(\omega_c-\omega_m)t} + a_i e^{j[(\omega_c-\omega_r)t+\phi_i]}\} \\ &\quad + \hat{e}_y \cdot b e^{j[(\omega_c-\omega_r)t+\phi_r]}, \end{aligned} \tag{1}$$

where $\hat{e}_x$ and $\hat{e}_y$ denote the two orthogonally polarization states and a_s, a_m, a_i, and b represent the optical amplitudes. ϕ_i and ϕ_r are the phases introduced by the initial phase difference and the transmission paths difference. The optical signal in Eq. (1) is injected into the signal port of a polarization-multiplexed 90° optical hybrid.

The other part of the optical carrier is injected into another CS-OSSB modulator, at which the LO signal with a frequency of ω_L is modulated. The optically carried LO signal expressed as $E_{\mathrm{LO}} = ce^{j(\omega c-\omega L)}$ is injected to the LO port of the polarization-multiplexed 90° optical hybrid. 0, π, $\pi/2$, $3\pi/2$ phase shifts are introduced by the polarization-multiplexed 90° optical hybrid between the optically carried LO signal and the optically carried RF signal. Two in-phase ($I_{1x,y} \propto \hat{e}_{x,y}E_{\mathrm{RF}x,y} + \hat{e}_{x,y}E_{\mathrm{LO}}$, $I_{2x,y} \propto \hat{e}_{x,y}E_{\mathrm{RF}x,y} - \hat{e}_{x,y}E_{\mathrm{LO}}$) and two quadrature ($Q_{1x,y} \propto \hat{e}_{x,y}E_{\mathrm{RF}x,y} + j\hat{e}_{x,y}E_{\mathrm{LO}}$, $Q_{2x,y} \propto \hat{e}_{x,y}E_{\mathrm{RF}x,y} - j\hat{e}_{x,y}E_{\mathrm{LO}}$) optical outputs are obtained along the two orthogonal polarization axes of $\hat{e}_x$ and $\hat{e}_y$, respectively. A π-phase difference of the photonic LO is introduced for the two in-phase (I_{1x} and I_{2y}) and the two quadrature (Q_{1x} and Q_{2y}) optical outputs with orthogonal polarization states. Power weighting and time delay of the cancellation reference signal for self-interference cancellation are realized in the optical domain through tuning the variable optical attenuators (VOAs) and the optical tunable delay lines (OTDLs) in I_{2y} and Q_{2y} paths. After optical-to-electrical conversion at the photodetectors (PDs), the electrical outputs can be expressed as

$$\begin{cases} i_{I_{1x}} \propto \Re_{I_{1x}}\eta_{I_{1x}}\{a_s c \cos[(\omega_s-\omega_L)t+\theta_{I_{1x}}] \\ +a_m c \cos[(\omega_L-\omega_m)t+\theta_{I_{1x}}] + a_i c \cos[(\omega_r-\omega_L)t+(\phi_i+\theta_{I_{1x}})]\} \\ i_{Q_{1x}} \propto \Re_{Q_{1x}}\eta_{Q_{1x}}\{-a_s c \sin[(\omega_s-\omega_L)t+\theta_{Q_{1x}}] \\ +a_m c \sin[(\omega_L-\omega_m)t+\theta_{Q_{1x}}] - a_i c \sin[(\omega_r-\omega_L)t+(\phi_i+\theta_{Q_{1x}})]\} \\ i_{I_{2y}} \propto -\Re_{I_{2y}}\eta_{I_{2y}} bc \cos[(\omega_r-\omega_L)t+(\phi_r+\theta_{I_{2y}})] \\ i_{Q_{2y}} \propto \Re_{Q_{2y}}\eta_{Q_{2y}} bc \sin[(\omega_r-\omega_L)t+(\phi_r+\theta_{Q_{2y}})] \end{cases}, \tag{2}$$

where η represents the power attenuation coefficients of the VOAs, θ represents the phases introduced by the OTDLs, and $\Re$ represents the responsivities of the PDs, respectively. By properly tuning the OTDLs to make $\phi_i + \theta_{I1x} = \phi_r + \theta_{I2y}$, $\theta_{I1x} = \theta_{Q1x}$, $\theta_{I2y} = \theta_{Q2y}$, the phase inversion between the downconverted self-interference component in i_{I1x} (or i_{Q1x}) and the downconverted reference signal component at the frequency of $|\omega_r - \omega_L|$ in i_{I2y} (or i_{Q2y}) is achieved. By combining i_{I1x} and i_{Q1x} (or i_{I2y} and i_{Q2y}) through an electrical 90° hybrid, respectively, the outputs are given by

$$\begin{cases} i_1 = i_{I_{1x}}\angle\frac{\pi}{2} + i_{Q_{1x}}\angle 0 \\ = -\Re_{I_{1x}}\eta_{I_{1x}}a_s c\ \sin[(\omega_s - \omega_L)t + \theta_{I_{1x}}] - \Re_{Q_{1x}}\eta_{Q_{1x}}a_s c\ \sin[(\omega_s - \omega_L)t + \theta_{Q_{1x}}] \\ -\Re_{I_{1x}}\eta_{I_{1x}}a_m c\ \sin[(\omega_L - \omega_m)t + \theta_{I_{1x}}] + \Re_{Q_{1x}}\eta_{Q_{1x}}a_m c\ \sin[(\omega_L - \omega_m)t + \theta_{Q_{1x}}] \\ -\Re_{I_{1x}}\eta_{I_{1x}}a_i c\ \sin[(\omega_r - \omega_L)t + (\phi_i + \theta_{I_{1x}})] - \Re_{Q_{1x}}\eta_{Q_{1x}}a_i c\ \sin[(\omega_r - \omega_L)t + (\phi_i + \theta_{Q_{1x}})] \\ i_2 = i_{I_{2y}}\angle\frac{\pi}{2} + i_{Q_{2y}}\angle 0 \\ = \Re_{I_{2y}}\eta_{I_{2y}}bc\ \sin[(\omega_r - \omega_L)t + (\phi_r + \theta_{I_{2y}})] + \Re_{Q_{2y}}\eta_{Q_{2y}}bc\ \sin[(\omega_r - \omega_L)t + (\phi_r + \theta_{Q_{2y}})] \end{cases}. \quad (3)$$

As can be seen, by properly tuning the VOAs to make $\Re_{I1x}\eta_{I1x}a_i = \Re_{I2y}\eta_{I2y}b = \Re_{Q1x}\eta_{Q1x}a_i = \Re_{Q2y}\eta_{Q2y}b$, the downconverted image at $|\omega_m - \omega_L|$ will be eliminated, while the downconverted signal of interest at $|\omega_s - \omega_L|$ will be enhanced. Equation (3) can be rewritten as

$$\begin{cases} i_1 = -2\Re_{I_{1x}}\eta_{I_{1x}}a_s c\ \sin[(\omega_s - \omega_L)t + \theta_{I_{1x}}] \\ -2\Re_{I_{1x}}\eta_{I_{1x}}a_i c\ \sin[(\omega_r - \omega_L)t + (\phi_i + \theta_{I_{1x}})] \\ i_2 = 2\Re_{I_{2y}}\eta_{I_{2y}}bc\ \sin[(\omega_r - \omega_L)t + (\phi_r + \theta_{I_{2y}})] \end{cases}. \quad (4)$$

By combining the electrical outputs given in Eq. (4), the downconverted self-interference at $|\omega_r - \omega_L|$ will be canceled. The final electrical output can be written as $i \propto -2\Re_{I1x}\eta_{I1x}a_s c \cdot \sin[(\omega_s - \omega_L)t + \theta_{I1x}]$. It can be seen only when the wanted IF signal at $|\omega_s - \omega_L|$ downconverted from the signal of interest is obtained. Thus, simultaneous self-interference cancellation and image-reject mixing are achieved. It should be noticed that the two electrical hybrids and one electrical coupler used here operate with the downconverted signals; thus, the influence with the working frequency of the whole system is low.

An experiment based on the scheme shown in Fig. 1 is performed. An optical carrier is generated from a laser diode (LD, Teraxion NLL) with the wavelength and the power set to 1550.12 nm and 16 dBm, respectively. The light wave is divided into two parts with equal power through a 3 dB optical coupler. The dual-polarization CS-OSSB modulator is realized by using a dual-polarization quadrature phase-shift keying (DP-QPSK) modulator consisting of two integrated polarization multiplexed dual-parallel Mach–Zehnder modulators (DP-MZMs). The DP-QPSK modulator (Fujitsu FTM7977) has a bandwidth of 23 GHz. The CS-OSSB modulator to modulate the LO signal is realized by a MZM together with an optical filter to select one desired sideband. The MZM (Fujitsu FTM7938) has a bandwidth of 40 GHz. Two EDFAs (Amonics AEDFA-35-B-FA) are introduced in the two branches to ensure the proper optical power level injecting into the 90° optical hybrid. The RF signals are generated by a microwave signal source (Agilent N5183B, 9 kHz–20 GHz) and an arbitrary waveform generator (AWG, Keysight M8195A, 65 GSa/s). The LO signal is generated from another microwave signal source (Anapico APSIN20G, 100 kHz–20 GHz). The polarization-multiplexed 90° optical hybrid (Kylia COH28) has a phase accuracy of 2°. The PDs (GD45216S) have a 3 dB bandwidth of 20 GHz and a responsivity of 0.65 A/W. The OTDLs (General Photonics) have a time delay tuning range of 600 ps. An electrical spectrum analyzer (ESA, Agilent N9010A) with a frequency range of 3 Hz–43 GHz is used to monitor the electrical spectra.

The performance of the proposed scheme is investigated. A single-tone signal at 10 GHz with a power of 10 dBm is used as the signal of interest. The self-interference of a linear frequency modulated (LFM) signal centered at 10 GHz with a 100-MHz bandwidth is also injected with a power of 0 dBm. The LO signal at 8 GHz with a power of 20 dBm is used. The reference signal is set to be a LFM signal centered at 10 GHz with a 100-MHz bandwidth and a power of 0 dBm. The received RF signal (containing the signal of interest and the self-interference) and the reference signal are modulated at the two integrated polarization-multiplexed DP-MZMs of the DP-QPSK modulator, respectively, and the modulation format is set to be CS-OSSB modulation. In this way, the optically carried RF signal and the optically carried reference signal are along the two orthogonal polarization axes. When disconnecting I_{y2} and Q_{y2}, the output of the system without either self-interference cancellation or image-reject mixing is shown in Fig. 2(i-a). As can be seen, both the signal of interest and the self-interference are downconverted to a center frequency of 2 GHz. By connecting I_{y2} and Q_{y2}, the output electrical spectrum with the self-interference canceled is shown in Fig. 2(i-b). A self-interference cancellation depth of 35 dB is achieved over 100-MHz bandwidth. In order to show the image-rejection performance, the signal of interest is disconnected and switched

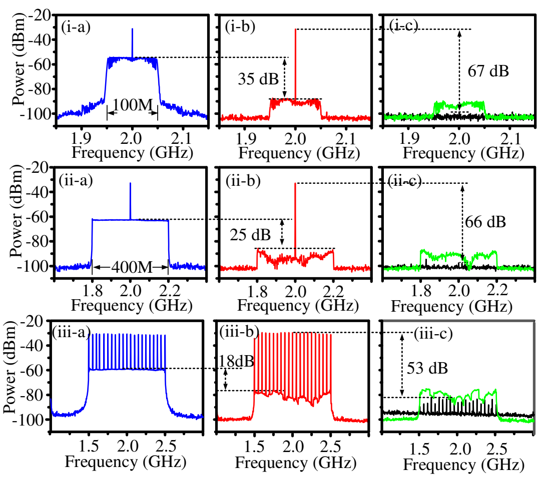

Fig. 2. Measured output electrical spectra (a) without either self-interference cancellation or image rejection, (b) with self-interference cancellation and image-reject mixing when the signal of interest is injected, or (c) with self-interference cancellation and image-reject mixing when the signal of interest switched to the corresponding image. The frequency of the LO signal is 8 GHz, and the self-interference has a center frequency of 10 GHz and a bandwidth of (i) 100 MHz, (ii) 400 MHz (here the signal of interest and the image is 10 and 6 GHz, respectively), and (iii) 1 GHz (here the signal of interest sweeps from 9.5 to 10.5 GHz, and the image sweeps from 6.5 to 5.5 GHz with a step of 50 MHz, respectively).

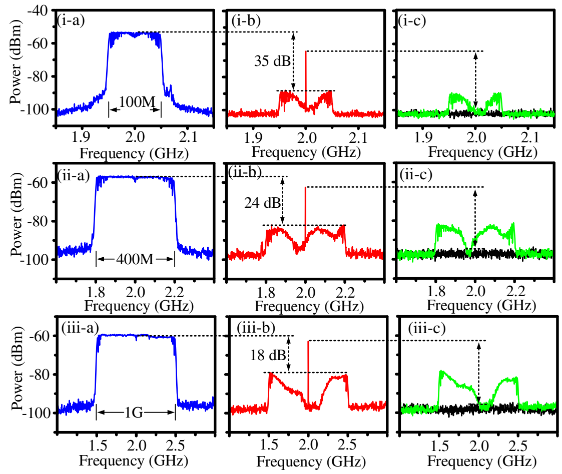

Fig. 3. Output electrical spectra (a) without either self-interference cancellation or image rejection, (b) with self-interference cancellation and image-reject mixing when the signal of interest is injected, or (c) with self-interference cancellation and image-reject mixing when the signal of interest switched to the corresponding image. The frequency of the LO signal is 14 GHz, the signal of interest and the image is 16 and 12 GHz with a power of −15 dBm, respectively, and the self-interference has a 16-GHz center frequency and a bandwidth of (i) 100 MHz, (ii) 400 MHz, and (iii) 1 GHz.

to the corresponding image at 6 GHz with a 10-dBm power. The output electrical spectrum is shown as the green solid line in Fig. 2(i-c). As can be seen, the downconverted image is suppressed to be lower than the canceled self-interference. In order to show the exact image-rejection ratio, the self-interference signal is disconnected, and the output electrical spectrum is shown as the black solid line in Fig. 2(i-c). An image-rejection ratio of 67 dB is obtained. Then, the bandwidth of the self-interference signal changes to be 400 MHz. The corresponding self-interference cancellation and image-reject mixing performances are shown in Fig. 2(ii). As can be seen, the self-interference cancellation depth of 25 dB over 400-MHz bandwidth has been achieved. The image-rejection ratio of 66 dB is guaranteed. Furthermore, in order to investigate the wideband performance, the signal of interest sweeps from 9.5 to 10.5 GHz, and the image sweeps from 6.5 to 5.5 GHz with a step of 50 MHz, respectively. The self-interference has a center frequency of 10 GHz and a bandwidth of 1 GHz. The system performance is shown in Fig. 2(iii). As can be seen, the self-interference cancellation depth of 18 dB and the image-rejection ratio of 53 dB over 1-GHz bandwidth have been achieved.

The system performances at different frequencies and different powers are also investigated. Both the frequency of the signal of interest and the center frequency of the self-interference are tuned to be 16 GHz in the Ku band. The LO signal changes to be 14 GHz, and the corresponding image changes to be 12 GHz. The power of the LFM signal is kept to be 0 dBm, while the powers of the signal of interest and the image change to be −15 dBm. The self-interference cancellation and image-reject mixing performances are shown in Fig. 3. As can be seen, the self-interference depth of 35 dB over 100-MHz bandwidth, 24 dB over 400-MHz bandwidth, and 18 dB over 1-GHz bandwidth can still be guaranteed. In addition, the image has also been suppressed to be under the noise level for all the cases.

The operational frequency of the system is mainly limited by the bandwidth of the DP-QPSK modulator, which can be further improved if a modulator with a larger bandwidth is available. The image-reject ratio of this approach over a wide bandwidth should be further improved. The self-interference cancellation ratio and the image-rejection ratio are mainly limited by the phase accuracies of the 90° optical hybrid and the electrical hybrids. Therefore, the system performance can be further improved if 90° optical and electrical hybrids with higher phase accuracies are used. In addition, the system stability can be further improved by using polarization-maintained devices and packaging the whole system.

In conclusion, a photonic approach to realize simultaneous self-interference cancellation and image-reject mixing is proposed and demonstrated. By using only one polarization-multiplexed 90° optical hybrid, all the operations of phase shift, time delay, and power weighting required by the two functions are realized using optical methods. The proposed approach can find applications in RF systems such as radar, electronic warfare, and wireless communication to improve the system spectral efficiencies and to enable the in-band full-duplex operations.

Funding. National Natural Science Foundation of China (61971222); Jiangsu Provincial Program for High-Level Talents in Six Areas (DZXX-030); Jiangsu Province “333” Project (BRA2018042); Fundamental Research Funds for the Central Universities (NC2018005, NE2017002).

Disclosures. The authors declare no conflicts of interest.

REFERENCES

1. V. Raj, I. Dias, T. Tholeti, and S. Kalyani, IEEE J. Sel. Top. Signal Process. **12**, 20 (2018).
2. M. Ozger, F. Alagoz, and O. B. Akan, IEEE Commun. Mag. **56**(4), 156 (2018).
3. S. L. Pan, D. Zhu, S. F. Liu, K. Xu, Y. T. Dai, T. L. Wang, J. G. Liu, N. H. Zhu, Y. Xue, and N. J. Liu, IEEE Microwave Mag. **16**(8), 61 (2015).
4. Z. Zhang, X. Chai, K. Long, A. V. Vasilakos, and L. Hanzo, IEEE Commun. Mag. **53**(5), 128 (2015).
5. Z. Li, Y. Xia, W. Pei, K. Wang, and D. P. Mandic, IEEE Trans. Signal Process. **66**, 4065 (2018).
6. A. Sabharwal, P. Schniter, D. Guo, D. W. Bliss, S. Rangarajan, and R. Wichman, IEEE J. Sel. Areas Commun. **32**, 1637 (2014).
7. D. Zhu and S. L. Pan, Photonics **5**, 6 (2018).
8. M. Lu, M. Chang, Y. Deng, and P. Prucnal, Appl. Opt. **52**, 2484 (2013).
9. Q. Zhou, H. Feng, G. Scott, and M. P. Fok, Opt. Lett. **39**, 6537 (2014).
10. M. P. Chang, M. Fok, A. Hofmaier, and P. R. Prucnal, IEEE Microwave Wireless Compon. Lett. **23**, 99 (2013).
11. J. Suarez, K. Kravtsov, and P. R. Prucnal, IEEE J. Quantum Electron. **45**, 402 (2009).
12. X. Han, B. Huo, Y. Shao, C. Wang, and M. Zhao, IEEE Photon. Technol. Lett. **29**, 917 (2017).
13. Y. Xiang, G. Li, and S. Pan, Opt. Express **25**, 21259 (2017).
14. Z. Z. Tang and S. L. Pan, IEEE Trans. Microwave Theory Tech. **64**, 3017 (2016).
15. D. Zhu, W. J. Chen, and S. L. Pan, Opt. Express **26**, 28022 (2018).
16. Y. Gao, A. Wen, W. Chen, and X. Li, Opt. Lett. **42**, 1105 (2017).
17. D. Shan, A. Wen, W. Zhai, X. Li, W. Zhang, and Z. Tu, Appl. Opt. **58**, 3432 (2019).
18. W. J. Chen, D. Zhu, C. X. Xie, J. Liu, and S. L. Pan, Opt. Lett. **44**, 4052 (2019).
19. B. Weng, Y. Chen, and Y. Chen, Appl. Opt. **58**, 3539 (2019).
20. X. P. Hu, D. Zhu, W. J. Chen, D. Ben, and S. L. Pan, “Photonic simultaneous self-interference cancellation and image-reject mixing,” ACP (to be published).